Investigation of the effect of iron nanoparticles on n-dodecane combustion under external electrostatic fields - Supporting Information

Efstratios Kritikos[a,*], Andrea Giusti[a]

[a] *Department of Mechanical Engineering, Imperial College London, South Kensington Campus, London SW7 2AZ, United Kingdom*

*e.kritikos19@imperial.ac.uk

Abstract

This document reports additional information in support of the description of the method and discussion of the results presented in the main paper.

S1. Modelling of atomic charges under external electrostatic fields

In this study the Charge Transfer with Polarization Current Equalization (QTPIE) method was used for the computation of the charge distribution inside the domain. For a detailed description of the method the reader is referred to Refs. [1–4]. The primitive Gaussian Type Orbitals (GTO) are used to compute the overlap integrals. The overlap integral ϕ between two Gaussian s functions is given by [5]:

$$\phi_{AB} = \left(\frac{\pi}{a+b}\right)^{3/2} \exp\left[-\frac{ab}{a+b} R_{AB}\right], \tag{1}$$

where a, b are the Gaussian exponents of the two atoms A, B, and R_{AB} is their interatomic distance. From the above expression, the distance d_s where the integral becomes smaller than 10^{-k} can be derived [5]. d_s is given by

$$d_s = \sqrt{\alpha^{-1} \log\left[\left(\frac{\pi}{2\alpha}\right)^3 10^{2k}\right]}. \tag{2}$$

The values of the Gaussian type exponents are computed from the Slater type exponents of the ReaxFF FeCHO-2016 for each species. Specifically, a fitting of the exponents of s-type primitive Gaussian orbitals is performed in order the two-electron Coulomb integrals to match those of the s-type Slater orbitals. The tolerance of the fitting is set to 10^{-16}. The aforementioned procedure is analytically described in Ref. [3]. The fitted values are given in Table S1.

Table S1: Species parameters used in this study.

Element	χ [eV][a]	η [eV][a]	α [a.u.][b]	d_s [Å] for $k = 5$
Fe	1.779	8.628	0.079	10.64
C	4.845	7.000	0.227	5.96
H	3.725	9.609	0.609	3.45
O	8.500	8.312	0.238	5.80

[a]based on the ReaxFF FeCHO-2016, [b]after performing the fitting

S2. Polarization of an isolated nanoparticle

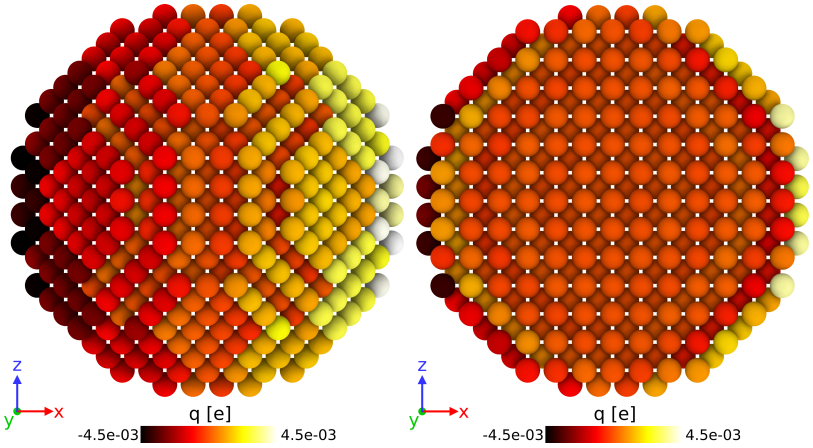


Fig. S1: Atomic charges of a polarized Iron Nanoparticle (FeNP) (left) and a slice of that FeNP (right) with BCC structure and a lattice parameter of $a = 2.866$ Å under a 0.1 V/Å external Electric Field (EF) in the x-direction.

S3. Preparation of the amorphous nanoparticle

A large Body-Centered Cubic (BCC) crystal is created with a lattice constant of 2.866 Å [6]. Afterwards, a sphere with a 40 Å diameter is extracted from the crystal to create the nanoparticle. The nanoparticle is then energy minimized with a conjugate gradient method to obtain a minimum potential energy state. Then velocities are assigned for each atom based on a Maxwell-Boltzmann (MB) distribution at a room temperature of 298.15 K. The structure is relaxed for 200 fs using a 0.2 fs timestep. Subsequently, the nanoparticle is heated at a rate of 1.7 K/ps till its temperature reaches 2000 K. After the 2000 K temperature is reached, a cooling process follows for 50 ps with a 10 K/ps cooling rate. Therefore, the nanoparticle reaches a temperature of 1500 K. At this point the nanoparticle, n-dodecane and oxygen molecules are inserted in a domain at the given densities. A timestep of 0.1 fs is applied. Random initial velocities are assigned to the atoms sampled from a MB distribution at 1500 K and the system is equilibrated for a total duration of 0.5 ns. During the equilibration process the Fe–C, Fe–H, Fe–O, C–O and H–O bonds are switched off to avoid any reactions from taking place during this step. After the system is equilibrated, it is rapidly heated till the simulation temperature with a heating rate of 10 K/ps. The relaxation, heating, cooling and equilibration stages are performed using the canonical NVT ensemble. The Nosé-Hoover thermostat is applied to keep the temperature constant with a damping parameter of 100 fs. At the end of the heating process all bonds are switched on again and the appropriate ensemble is applied. Additionally, the external EFs are activated.

S4. Charge distribution under different charge equilibration methods

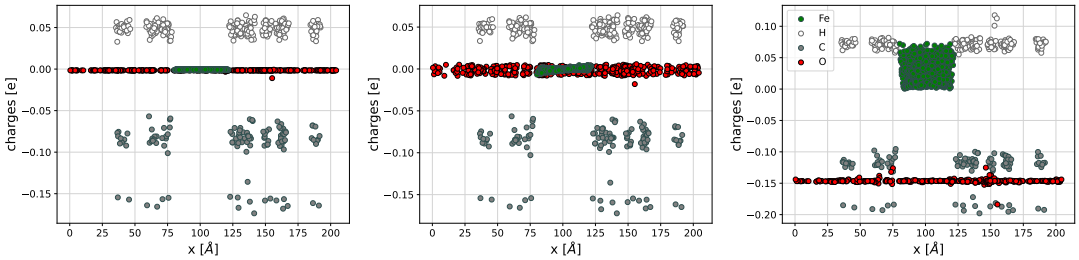


Fig. S2: (left) QTPIE at 0 V/Å, (middle) QTPIE at 0.1 V/Å and (right) Charge Equilibration (QEq) at 0 V/Å at timestep 0 after the heating stage; no reactions have occurred; thus, all Fe atoms belong to the FeNP, all O atoms belong to oxygen molecules and all C, H atoms belong to n-dodecane molecules.

S5. Activation energies of selected reactions

In order to evaluate the suitability of the ReaxFF FeCHO-2016 force field in the study of n-dodecane combustion, the activation energies of selected hydrocarbon and oxygen compound reactions are computed. The Minimum Energy Path (MEP) of reactions is found by performing Nudged Elastic Band (NEB) computations [7] with the Climbing Image (CI) [8] method. The NEB analysis is based on the simultaneous minimization of intermediate images along the energy path of a reaction. The position of the images along the transition path is fixed by applying a spring force. After this minimization process, the image with the highest energy further climbs the potential energy surface until a saddle point is reached. This saddle point should correspond to the activation energy of the reaction. All NEB computations were performed in LAMMPS [9]. The number of images was set to 6 and a spring force of 1 kcal/(mol·Å) was applied between adjacent images. Results are presented in Table S2 for various reactions. A comparison was also made with the ReaxFF CHO-2016 [10]. The activation energy results appear to be in good agreement with the literature. Nonetheless, an approximately 10% increase in the activation energies computed with the ReaxFF FeCHO-2016 compared to the ReaxFF CHO-2016 is noted.

Table S2: Activation energy of n-dodecane pyrolysis reactions and oxygen compound reactions, in kcal/mol, without an external EF

(a) C–C bond β-scission

Reaction	ReaxFF FeCHO-2016	ReaxFF CHO-2016	Ref. [11]	Ref. [12]
n-$C_{12}H_{26} \rightarrow$ n-$C_{11}H_{23}$ + n-CH_3	84.02	81.14	86.52	81.78, 88.93
n-$C_{12}H_{26} \rightarrow$ n-$C_{10}H_{21}$ + n-C_2H_5	77.79	76.06	86.28	77.66, 85.97
n-$C_{12}H_{26} \rightarrow$ n-C_9H_{19} + n-C_3H_7	78.63	76.90	87.48	77.22, 85.59
n-$C_{12}H_{26} \rightarrow$ n-C_8H_{17} + n-C_4H_9	78.12	76.00	87.24	77.64, 85.44
n-$C_{12}H_{26} \rightarrow$ n-C_7H_{15} + n-C_5H_{11}	84.32	76.36	87.48	77.07, 84.56
n-$C_{12}H_{26} \rightarrow$ 2 n-C_6H_{13}	84.02	76.14	87.48	77.03, 84.34

(b) H abstraction reactions (brackets correspond to the atomic ids of Figure S3)

Reaction	ReaxFF FeCHO-2016	ReaxFF CHO-2016	Ref. [11]	Ref. [12]
n-$C_{12}H_{26} \rightarrow$ n-$CH_3(CH_2)_{10}CH_2$ + H [H13]	96.17	93.86	99.90$^{\alpha}$	98.57, 101.55$^{\alpha}$
n-$C_{12}H_{26} \rightarrow$ n-$CH_3(CH_2)_{10}CH_2$ + H [H14]	98.04	94.46	99.90$^{\alpha}$	98.57, 101.55$^{\alpha}$
n-$C_{12}H_{26} \rightarrow$ n-$CH_3(CH_2)_9CH{\cdot}CH_3$ + H	97.28	87.62	97.04	94.28, 97.38
n-$C_{12}H_{26} \rightarrow$ n-$CH_3(CH_2)_8CH{\cdot}CH_2CH_3$ + H	91.83	88.50	97.28	94.26, 97.19
n-$C_{12}H_{26} \rightarrow$ n-$CH_3(CH_2)_7CH{\cdot}(CH_2)_2CH_3$ + H	91.61	87.37	97.28	93.75, 96.74
n-$C_{12}H_{26} \rightarrow$ n-$CH_3(CH_2)_6CH{\cdot}(CH_2)_3CH_3$ + H	96.31	87.88	97.28	93.80, 96.60
n-$C_{12}H_{26} \rightarrow$ n-$CH_3(CH_2)_5CH{\cdot}(CH_2)_4CH_3$ + H	98.30	87.68	97.28	94.28, 97.14

$^{\alpha}$ A single value is reported for C–H bond scission of the methyl group

(c) oxygen compound reaction

Reaction	ReaxFF FeCHO-2016	ReaxFF CHO-2016	Ref. [13]
$H_2O \rightarrow H_2 + O$	117.99	106.49	113 – 119

(d) Dissociation of oxygen

Reaction	ReaxFF FeCHO-2016	ReaxFF CHO-2016	Ref. [14]
$O_2 \rightarrow 2O$	124.0	116.8	118.7

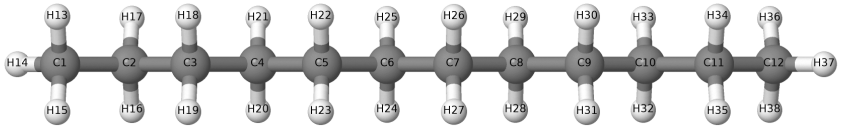


Fig. S3: Atomic labels of an n-dodecane molecule.

S6. Initiation time of fuel and oxidizer absorption

Table S3: Initiation time in picoseconds of fuel and oxidizer absorption under (a) 0 V/Å and (b) 0.1 V/Å EF.

(a) $\mathcal{E} = 0$ V/Å

Ensemble	Density [kg/m^3]	Temperature [K]	$t_{init.}$ of n-$C_{12}H_{26}$	$t_{init.}$ of O_2
NVT	81.2	1800	3.3	0.3
NVT	31.7	1800	9.2	8.3
NVT	31.7	2000	0.3	2.0
NVE	81.2	1800	4.3	0.3
NVE	31.7	1800	10.2	7.1
NVE	31.7	2000	0.3	6.5

(b) $\mathcal{E} = 0.1$ V/Å

Ensemble	Density [kg/m^3]	Temperature [K]	$t_{init.}$ of n-$C_{12}H_{26}$	$t_{init.}$ of O_2
NVT	81.2	1800	3.5	0.2
NVT	31.7	1800	26.2	12.5
NVT	31.7	2000	0.3	6.9
NVE	81.2	1800	6.5	0.3
NVE	31.7	1800	25.3	2.2
NVE	31.7	2000	0.5	2

S7. Number of molecules of products

Table S4: Number of molecules of products for the (a) NVT and (b) NVE simulations for 31.7 kg/m^3 and 1800 K condition, averaged over consecutive time periods of 500 ps (i.e., $\tau_1 = \tau_2 = \tau_3 = \tau_4 = 500$ ps).

(a) NVT simulations

Species	Electric field [V/Å]											
	0				1e-4				1e-3			
	τ_1	τ_2	τ_3	τ_4	τ_1	τ_2	τ_3	τ_4	τ_1	τ_2	τ_3	τ_4
HO_2	1.1e-4	0.0	0.0	2.2e-4	0.0	0.0	0.0	0.0	1.2e-4	0.0	0.0	0.0
CO_2	0.0	0.0	0.0	0.0	0.0	0.0	0.0	0.0	0.0	0.0	0.0	0.0
C_nH_m	2.1e-4	1.6e-4	0.0	0.0	7.6e-4	6.5e-4	5.4e-5	0.0	4.2e-4	0.0	0.0	1.1e-4
OH	2.7e-2	8.2e-4	9.3e-4	8.7e-4	1.1e-4	7.1e-4	8.6e-4	1.6e-1	4.6e-4	7.5e-4	6.1e-2	3.0e-1
CO	0.0	0.0	0.0	0.0	0.0	0.0	0.0	0.0	0.0	0.0	0.0	0.0
H_2O	7.3e0	2.4e1	3.7e1	4.6e1	8.2e0	2.7e1	4.4e1	4.5e1	8.4e0	2.8e1	3.2e1	3.5e1
H_2	1.7e1	3.3e1	3.9e1	4.0e1	1.5e1	3.3e1	4.0e1	4.0e1	2.5e1	4.1e1	4.2e1	4.0e1
$Fe_kC_nH_mO_p$	4.4e-4	5.4e-4	2.0e-1	3.5e-1	3.6e-4	4.7e-1	6.7e-1	6.5e-1	2.3e-4	2.0e-1	3.3e-1	3.4e-1

Species	Electric field [V/Å]							
	1e-2				0.1			
	τ_1	τ_2	τ_3	τ_4	τ_1	τ_2	τ_3	τ_4
HO_2	0.0	6.3e-5	0.0	0.0	9.9e-2	5.6e-2	9.3e-2	5.9e-2
CO_2	0.0	0.0	0.0	0.0	0.0	0.0	1.2e-1	4.0e-4
C_nH_m	5.4e-4	2.3e-4	0.0	0.0	1.2e0	3.8e-1	0.0	0.0
OH	2.3e-4	6.0e-4	8.8e-4	6.1e-4	3.5e-1	2.3e0	3.9e0	3.6e0
CO	0.0	0.0	0.0	0.0	1.5e-1	8.3e-1	8.1e-1	7.3e-1
H_2O	1.0e1	3.3e1	3.4e1	3.5e1	1.0e1	2.7e1	2.4e1	2.2e1
H_2	3.1e1	5.9e1	6.2e1	5.9e1	2.0e1	3.9e1	3.8e1	3.4e1
$Fe_kC_nH_mO_p$	5.5e-4	8.6e-4	2.5e-1	3.4e-1	2.9e-4	2.7e-1	5.9e-1	6.1e-1

(b) NVE simulations

Species	Electric field [V/Å]								
	0			1e-4			1e-3		
	τ_1	τ_2	τ_3	τ_1	τ_2	τ_3	τ_1	τ_2	τ_3
HO_2	2.7e-4	8.9e-5	4.4e-4	0.0	0.0	6.7e-5	8.3e-5	0.0	2.0e-1
CO_2	0.0	0.0	0.0	0.0	0.0	0.0	0.0	0.0	0.0
C_nH_m	3.6e-4	1.3e-4	1.5e-4	2.2e-4	2.0e-4	0.0	1.2e-3	2.5e-4	2.9e-4
OH	2.8e-4	2.1e-1	2.0e-2	1.6e-4	7.7e-2	1.7e-1	3.2e-4	3.2e-1	8.0e-2
CO	0.0	0.0	0.0	0.0	0.0	0.0	0.0	0.0	0.0
H_2O	3.9e0	2.0e1	2.9e1	4.0e0	2.1e1	3.5e1	4.0e0	1.9e1	3.2e1
H_2	1.6e1	4.5e1	5.6e1	1.4e1	4.1e1	5.3e1	1.7e1	3.7e1	4.5e1
$Fe_kC_nH_mO_p$	6.4e-5	5.9e-1	1.2e0	6.7e-5	2.2e-1	3.4e-1	4.7e-4	2.1e-2	4.5e-1

Species	Electric field [V/Å]					
	1e-2			0.1		
	τ_1	τ_2	τ_3	τ_1	τ_2	τ_3
HO_2	0.0	7.5e-4	0.0	1.4e-1	9.3e-2	1.1e-2
CO_2	0.0	0.0	0.0	1.0e-1	6.6e-2	5.7e-3
C_nH_m	4.1e-4	4.9e-4	0.0	2.7e0	2.1e-1	1.8e-1
OH	4.2e-4	7.4e-4	2.2e-3	1.3e0	1.1e1	1.3e1
CO	0.0	0.0	0.0	1.1e0	4.0e0	2.0e1
H_2O	5.9e0	2.5e1	2.9e1	1.1e1	8.3e0	1.2e0
H_2	2.6e1	6.4e1	6.9e1	4.7e1	4.6e1	1.9e1
$Fe_kC_nH_mO_p$	4.0e-4	1.5e-3	1.5e-1	6.8e-1	1.9e2	1.2e3

S8. Kinetic energy components

Table S5: Kinetic energy components in kcal/mol from (a) NVT and (b) NVE simulations for 31.7 kg/m^3 and 1800 K condition, averaged over the last nanosecond of the total simulated time.

(a) NVT simulations

KE	Electric field [V/Å]									
	0		1e-4		1e-3		1e-2		0.1	
	total	FeNP	total	FeNP	total	FeNP	total	FeNP	total	FeNP
KE_{tr}	753	0.10	777	0.09	695	0.19	1177	1.45	4964	25.81
KE_{rot}	639	5.64	662	5.57	624	5.59	778	5.39	844	3.99
KE_{vib}	17331	16869	17285	16859	17412	16969	16768	16540	12931	12416

(b) NVE simulations

KE	Electric field [V/Å]									
	0		1e-4		1e-3		1e-2		0.1	
	total	FeNP	total	FeNP	total	FeNP	total	FeNP	total	FeNP
KE_{tr}	1159	0.11	1206	0.2	1113	0.16	1566	0.69	21104	–
KE_{rot}	1007	6.36	1052	6.37	998	6.46	1160	6.55	6386	–
KE_{vib}	19587	19032	19380	18844	19791	19100	19864	19216	32289	–

S9. Temperature of the system

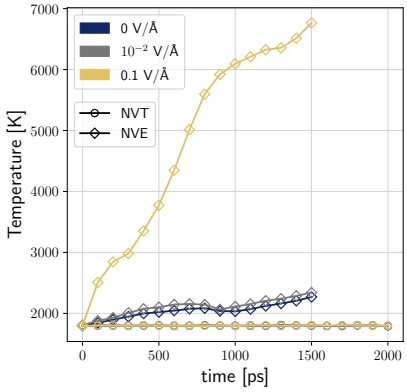


Fig. S4: System's temperature for the 31.7 kg/m^3 and 1800 K case.

S10. Time evolution of C, H atom bonds of an n-$C_{12}H_{26}$ molecule

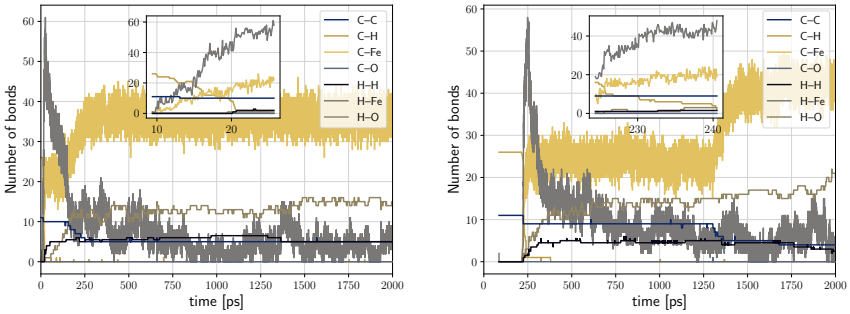


Fig. S5: Time evolution of C, H atom bonds of an n-$C_{12}H_{26}$ molecule without any EF (left) and with a 0.1 V/Å EF (right). Results are presented for NVT simulations at 31.7 kg/m^3 and 1800 K.

S11. Chemical composition of FeNP shell in NVE simulations

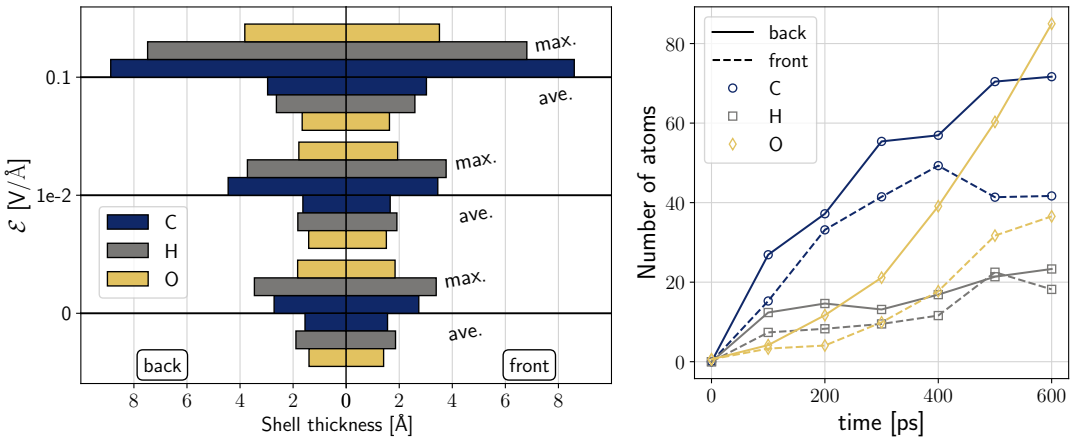


Fig. S6: Shell thickness for each species (top) and number of absorbed atoms in the FeNP at 0.1 V/Å (bottom); results are presented for NVE simulations for the 31.7 kg/m^3 and 1800 K condition. Note that since the FeNP fragments after 600 ps, results for shell thickness and number of absorbed atoms are presented untill 600 ps for all electric field cases.

References

[1] J. Chen, T. J. Martínez, QTPIE: Charge transfer with polarization current equalization. A fluctuating charge model with correct asymptotics, Chemical Physics Letters 438 (4-6) (2007) 315–320.

[2] J. Chen, D. Hundertmark, T. J. Martínez, A unified theoretical framework for fluctuating-charge models in atom-space and in bond-space, Journal of Chemical Physics 129 (21) (2008).

[3] J. Chen, T. J. Martínez, The Dissociation Catastrophe in Fluctuating-Charge Models and its Implications for the Concept of Atomic Electronegativity (2009) 397–415.

[4] J. Chen, Theory and applications of fluctuating-charge models, Ph.D. thesis, University of Illinois at Urbana-Champaign (2009).

[5] T. Helgaker, P. Jørgensen, J. Olsen, Molecular Electronic-Structure Theory, 2000.

[6] W. B. Pearson, A Handbook of Lattice Spacings and Structures of Metals and Alloys, Elsevier, 1958.

[7] G. Henkelman, H. Jónsson, Improved tangent estimate in the nudged elastic band method for finding minimum energy paths and saddle points, Journal of Chemical Physics 113 (22) (2000) 9978–9985.

[8] G. Henkelman, B. P. Uberuaga, H. Jónsson, A Climbing image nudged elastic band method for finding saddle points and minimum energy paths, Journal of Chemical Physics 113 (22) (2000) 9901–9904.

[9] S. Plimpton, Fast parallel algorithms for short-range molecular dynamics, Journal of Computational Physics (1995).

[10] C. Ashraf, A. C. Van Duin, Extension of the ReaxFF Combustion Force Field toward Syngas Combustion and Initial Oxidation Kinetics, Journal of Physical Chemistry A 121 (5) (2017) 1051–1068.

[11] L. Zhao, T. Yang, R. I. Kaiser, T. P. Troy, M. Ahmed, J. M. Ribeiro, D. Belisario-Lara, A. M. Mebel, Combined Experimental and Computational Study on the Unimolecular Decomposition of JP-8 Jet Fuel Surrogates. II: N-Dodecane (n-C12H26), Journal of Physical Chemistry A 121 (6) (2017) 1281–1297.

[12] Q. D. Wang, J. B. Wang, J. Q. Li, N. X. Tan, X. Y. Li, Reactive molecular dynamics simulation and chemical kinetic modeling of pyrolysis and combustion of n-dodecane, Combustion and Flame 158 (2) (2011) 217–226.

[13] O. Oldenberg, The Energy of Dissociation H $_2$ O→H+OH, The Journal of Chemical Physics 17 (11) (1949) 1059–1061. doi:10.1063/1.1747112.

[14] P. W. Atkins, J. De Paula, Atkins' Physical Chemistry, 8th Ed.; Oxford University Press (2018).